Mechanical properties of intermetallic compounds in the Au–Sn system

R.R. Chromik,[a] D-N. Wang, A. Shugar, L. Limata, M.R. Notis, and R.P. Vinci
Department of Materials Science and Engineering, Lehigh University, Whitaker Laboratory, Bethlehem, Pennsylvania 18015

(Received 5 January 2005; accepted 20 April 2005)

The mechanical properties of intermetallic compounds in the Au–Sn system were investigated by nanoindentation. Measurements of hardness and elastic modulus were obtained for all of the confirmed room-temperature intermetallics in this system as well as the β phase (8 at.% Sn) and $AuSn_4$. Overall, it was found that the Au–Sn compounds have lower hardness and stiffness than common Cu–Sn compounds found in solder joints. This finding is in contrast to common knowledge of "Au embrittlement" due to the formation of either $AuSn_4$ or $(Au,Ni)Sn_4$ intermetallic compounds. This difference in understanding of mechanical properties of these phases and the resulting joint strength is discussed in terms of reliability and possible failure mechanisms related to interface strength or microstructural effects. Indentation creep measurements performed on Au_5Sn, Au–Sn eutectic (29 at.% Sn) and AuSn indicate that these alloys are significantly more creep resistant than common soft solders, in keeping with typical observations of actual joint performance.

I. INTRODUCTION

Intermetallic compounds in the Au–Sn system have been of interest in joining applications for many decades.[1,2] During the advent of the microelectronics industry, eutectic Au–Sn solder (29 at.% Sn), with a melting point of 280 °C, was developed as a high temperature "first-attach" solder. This eutectic consists of two intermetallic compounds—Au_5Sn (ζ′) and AuSn (δ)—and is considered a relatively hard solder with superior creep resistance. Thus today, this solder is popular for optoelectonics applications where dimensional stability is critical.[3] In addition to their presence in Au–Sn eutectic solder, Au–Sn intermetallics also form with other Sn bearing solders (e.g., Pb–Sn and Sn–Ag–Cu) when Au is used as a finishing metal. In these cases, the formation of intermetallic compounds, primarily $AuSn_4$, has been tied to embrittlement and decreased reliability.[2,4–9] The most recent example of this phenomenon is the soldering of Pb–Sn to Au/Ni surface finishes.[6–8,10,11] In the work of Zribi et al.,[11,12] as-soldered joints were found to have acceptable strength. However, with solid state aging, a $(Au,Ni)Sn_4$ compound formed at the solder/Ni_3Sn_4 interface. The growth of this phase, observed even for submicron coatings of Au, was correlated to a decrease in joint strength and brittle failures.

Figure 1 is the equilibrium phase diagram for the Au–Sn system.[13,14] At room temperature, there are three confirmed stable intermetallic compounds: ζ′ (Au_5Sn), δ (AuSn), and ϵ ($AuSn_2$); there are also three others for which there is convincing experimental evidence of stability: β (8 at.% Sn), ζ (~10 at.% Sn), and η ($AuSn_4$). Despite claims of various mechanical benefits or drawbacks associated with the presence of Au in soldering, surprisingly few studies of the mechanical properties of Au–Sn compounds themselves exist in the literature.[15–18] Ghosh recently measured the elastic and plastic properties of $AuSn_4$ with resonance techniques and microhardness.[16] Vicenzo et al. performed nanoindentation on electrodeposited Au–Sn thick films. Most of their results are for metastable alloys, with a single measurement for crystalline AuSn (δ).[18] Yost et al.[15] measured the elastic properties of the Au_5Sn and AuSn intermetallics by resonance techniques, in addition to making measurements of coefficients of thermal expansion. Plastic properties of many of the Au-rich alloys were measured by Ciulik and Notis by microhardness.[17] Thus, among these four studies, there exist some mechanical-property data for most of the equilibrium intermetallic compounds, but no complete database of quasi-static behavior for alloys in the Au–Sn system, no consistency of experimental approach, and no creep data for individual phases. This limits the understanding of the role each intermetallic may play in determining solder joint performance and therefore limits the ability to efficiently design solder alloys, pad metallizations, and processes for maximum reliability.

The lack of mechanical-property data for Au–Sn

[a]Address all correspondence to this author.
Present address: U.S. Naval Research Laboratory, Code 6176, 4555 Overlook Ave. S.W., Washington, DC 20375.
e-mail: chromik@nrl.navy.mil
DOI: 10.1557/JMR.2005.0269

 © 2005 Materials Research Society

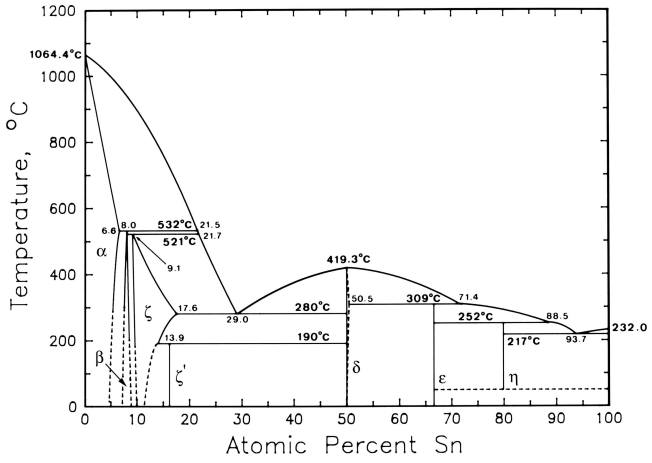

FIG. 1. Au–Sn phase diagram, adapted from Ciulik and Notis.[13,14]

compounds is partly due to the requirement for a bulk specimen for traditional mechanical testing techniques, such as compression/tension testing or resonance techniques. Preparation of large quantities of single phase alloys either requires specialized techniques[19] or long-term annealing of cast specimens.[16] These approaches are somewhat difficult to implement and may not yield specimens that are chemically and structurally representative of all possible intermetallics found in joints made using a certain solder alloy system. However, using nanoindentation, one can reliably measure the mechanical properties of intermetallic compounds common to soldering applications in diffusion couples aged for moderate times. This is due to the rapid interstitial diffusion for many noble metal species in Sn.[20,21] For example, in our recent study,[22] ageing of Cu/Sn and Ag/Sn diffusion couples for a few hundred hours at 200 °C produced intermetallic layers of 5 μm of more in thickness, sufficient for nanoindentation testing of Cu_3Sn, Cu_6Sn_5, and Ag_3Sn. More recently, two independent research groups, Deng et al.[23,24] and Jang et al.,[25] conducted similar nanoindentation experiments on Cu–Sn compounds and all observed good agreement for elastic modulus and hardness. Based on these studies, nanoindentation has been shown to be a quick, reliable technique for measuring the mechanical properties of intermetallic compounds at length scales similar to real solder joints. Measurements of the elastic (e.g., Young's modulus) and plastic properties of intermetallic compounds are necessary for finite element modeling of solder joints at a microstructural level,[26] where the nanoindentation hardness may be equated to a yield strength via Tabor's relation.[27]

For this investigation, the room-temperature elastic modulus, hardness, and short-time creep behavior of Au–Sn intermetallic compounds have been measured by nanoindentation. Samples were prepared as diffusion couples, with some bulk Au–Sn and Au–Ni–Sn alloys from other investigations also examined.[13,17,28] The quasi-static mechanical properties for all of the confirmed room temperature intermetallics (ζ′, δ, ϵ) are presented along with results for the β phase (8 at.% Sn), η ($AuSn_4$), and (Au,Ni)Sn_4. In addition, creep data for phases of interest in soldering with Au–Sn eutectic (29 at.% Sn) solder are also presented. The results are discussed in the context of the current understanding of the role of Au in soldering applications.

II. EXPERIMENT

Most of the Au–Sn intermetallics were fabricated by solid-state aging of diffusion couples. Due to the complexity of the Au–Sn phase diagram (compare Fig. 1) and the nature of competitive diffusion in the Au–Sn system,[29] it was necessary to prepare both an Au-rich and Sn-rich diffusion couple. The Au-rich couple consisted of a layer of pure Au (99.999+% purity) and a layer of Au–Sn eutectic solder (29 at.% Sn), while the Sn-rich couple was prepared with pure Au and pure Sn (99.985% purity). The diffusion couples were annealed at 185 °C, with anneal times of 48 h for the Sn-rich couple and 1 week for the Au-rich couple. These samples were then mounted in cross section in low viscosity epoxy and cured at room temperature. Standard metallographic techniques were used to prepare the specimens for subsequent microscopy and nanoindentation testing. The polishing schedule consisted of grinding with SiC paper down to a 15-μm-grit followed by polishing with 0.3-μm alumina and finally 0.05-μm colloidal silica.

Electron probe microanalysis (EPMA) was performed on the samples to identify specific phases and to measure the composition of each growth layer formed during annealing. A JEOL 733 probe (Tokyo, Japan) equipped with wavelength dispersive spectroscopy (WDS) was used for quantitative analysis. The accelerating voltage was 20 kV, and the probe current was maintained at 40 nA, with a 40 s peak and 20 s background counts. Standards for calibration of the microprobe were high-purity (99.999%) specimens of Au and Sn obtained from Geller (Topsfield, MA). The composition of each phase present in the alloys was determined by spot analysis with at least three analyses averaged for final quantitative values.

In addition to the diffusion couple samples prepared specifically for this study, two specimens were available from a previous study on the phase equilibria in the Au–Sn system[13,17] and a third specimen from a study on Au–Ni–Sn alloys.[28] The first specimen was a diffusion couple of pure Au and a Au-rich alloy of composition 10.0 at.% Sn that was annealed at 300 °C for 800 h. This diffusion couple sample was shown to contain the β phase (8 at.% Sn). The second specimen was a bulk single phase AuSn (δ) alloy (50.5 at.% Sn) that was

cast and annealed. The third specimen was a bulk $Au_{0.5}Ni_{0.5}Sn_4$ alloy prepared by casting and annealing.

Nanoindentation testing was carried out using a Triboscope 1D transducer (Hysitron, Minneapolis, MN) mounted to a Multimode atomic force microscope with a Nanoscope III controller (DI, Santa Barbara, CA). The Berkovich diamond tip (~150 nm defect radius) served both for indentation testing and as the atomic force microscope (AFM) tip during imaging. Pre-scanning of a specimen allowed for identification of interfaces within the diffusion couple samples. Based on these images and both optical and scanning electron microscopy characterization, the location of the tip with respect to the various phases in the diffusion couple could be determined. Often, preliminary indents were carried out within well-characterized materials such as pure Au or Sn, to verify the tip location prior to testing in the intermetallic compounds of interest. The indentation test consisted of three steps: a loading segment, at rates between 0.25 to 1.0 mN/s, to a maximum load between 0.7 and 9.5 mN, followed by a hold segment for 1–3 s, and finally, unloading at rates between 0.25 and 1.0 mN/s. The loading rates and hold segments were kept in these ranges whenever the hardness and elastic modulus were measured. However, for the $AuSn_4$ intermetallic, these rates were also varied from 0.01 to 2.0 mN/s to test for rate-dependent elastic (i.e., anelastic) effects. Also, when testing for creep behavior of Au_5Sn (ζ'), Au–Sn eutectic (29 at.% Sn) and AuSn (δ), the hold segment was increased to 5–10 s.

Measurements of the reduced modulus and hardness were carried out on all samples using the Oliver and Pharr method[30] in the same manner as in a previous report on Cu–Sn and Ag–Sn intermetallic compounds.[22] The area function of the diamond indenter was calibrated prior to testing by indenting a fused quartz reference material. The reduced modulus of a test material was calculated from a stiffness measurement obtained from the unloading slope and the area function for the diamond indenter. This reduced modulus E_r is defined by the elastic properties of both the sample and the indenter

$$E_r = \left(\left. \frac{1-\nu^2}{E} \right|_{sample} + \left. \frac{1-\nu^2}{E} \right|_{indenter} \right)^{-1} \quad , \qquad (1)$$

where E is Young's modulus and ν is Poisson's ratio. The properties of the diamond indenter are known ($E = 1140$ GPa and $\nu = 0.07$) and can be used to calculate an indentation modulus,

$$E_{NI} = \left. \frac{E}{1-\nu^2} \right|_{sample} \quad . \qquad (2)$$

Then, if Poisson's ratio of the test material is known, the Young's modulus may be calculated. Often, for common values of Poisson's ratio (0.25–0.35), the measured reduced modulus is quite close to a calculated Young's modulus.

The hardness of the sample is calculated from the standard definition

$$H_{NI} = \frac{P_{max}}{A(h_c)} \quad , \qquad (3)$$

where P_{max} is the maximum load of the test and $A(h_c)$ is the projected contact area.

Room-temperature creep measurements were performed on the Au_5Sn, Au–Sn eutectic, and AuSn samples. For measurements of creep during the constant load segment of nanoindentation testing, the strain rate is determined from

$$\dot{\epsilon} = \frac{1}{h}\frac{dh}{dt} \quad , \qquad (4)$$

where h is the indenter depth.[31,32] The hardness measurement is used as the average stress σ during this test, where the load is constant and the area changes as the indenter creeps into the specimen. The equation for secondary creep is used to plot creep curves relating the strain rate to the applied stress:

$$\dot{\epsilon} = C\sigma^n \quad , \qquad (5)$$

where C is a temperature dependent constant and n is the creep exponent. As observed in previous studies on indentation creep in solder type materials,[31–34] the use of Eq. 5 tends to yield large creep exponents for both short and long observation times, which may be due to an effect of transient creep on indentation experiments that is difficult to quantify.

For the bulk AuSn (δ), Vickers microindentation was also performed using a M-400FT hardness tester (LECO Corporation, St. Joseph, MN). Vickers hardness was calculated from the standard definition and then converted to a hardness value based on a projected contact area.[22] This conversion is convenient for comparisons, due to the fact that the Vickers and Berkovich indenter geometries have the same projected area versus depth relationship.[35]

III. RESULTS AND DISCUSSION

A. Sample characterization

The two diffusion couple samples prepared specifically for this study were examined by scanning electron microscopy (SEM) and EPMA to identify the compounds formed during annealing. Measurements of layer thicknesses were also carried out to provide a guide during nanoindentation testing. Figure 2 is a SEM image of

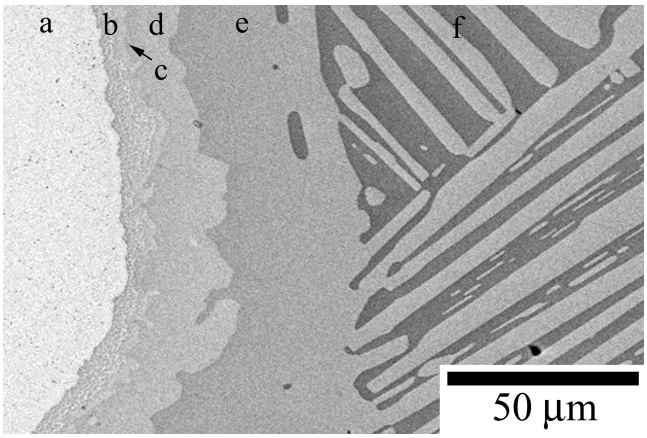

FIG. 2. Scanning electron microscopy image of the Sn-rich diffusion couple. Using electron probe microanalysis, the phases present in this sample were determined to be (a) Au, (b) Au_5Sn + AuSn, (c) AuSn, (d) $AuSn_2$, (e) $AuSn_4$, and (f) $AuSn_4$ + Sn.

the Sn rich diffusion couple. Two growth layers of the intermetallic compounds $AuSn_4$ and $AuSn_2$ were identified. Also, between the Au and $AuSn_2$, two layers were found: a very thin layer of AuSn next to the $AuSn_2$ and a layer exhibiting the eutectic structure consisting of Au_5Sn and AuSn. Based on Fig. 2 and measurements in this diffusion couple, the following materials were present at sufficient length scales for nanoindentation testing: Au, $AuSn_2$, $AuSn_4$, and Sn. Figure 3 is a SEM image of the Au-rich diffusion couple. One layer of intermetallic compound, Au_5Sn (ζ'), formed between Au and the eutectic solder (29 at.% Sn). The Au_5Sn phase consisted of a continuous layer and scallop-type growth extending into the solder. For this sample, nanoindentation testing was performed on Au, Au_5Sn, and the eutectic (AuSn + Au_5Sn).

B. Quasistatic nanoindentation

1. Au-rich and Sn-rich diffusion couples

Pre-scanning of the two new diffusion couple samples with the atomic force microscope mode of the TriboScope indenter allowed for identification of interfaces between various phases. Nanoindentation was then carried out, typically starting either in pure Au or pure Sn. These measurements on the pure elements were used to verify the indenter tip location in the diffusion couple. The tip was then moved across the interface between the pure element and the respective intermetallic compound. Post-scanning allowed for verification that the test was performed in the correct phase and away from interfaces. Similar to a previous study,[22] indents found to be less than 2 μm from an interface were not used in the final datasets. Although it has not been quantified, the interaction of the elastic-plastic strain field below the indenter with a boundary or a secondary phase can affect the nanoindentation results. This is similar to concerns about a substrate effect in thin films.[36,37] It was not rigorously studied how proximity to a phase boundary would affect our results, but based on the discarded data, there was no indication that boundary effects are influencing the data presented.

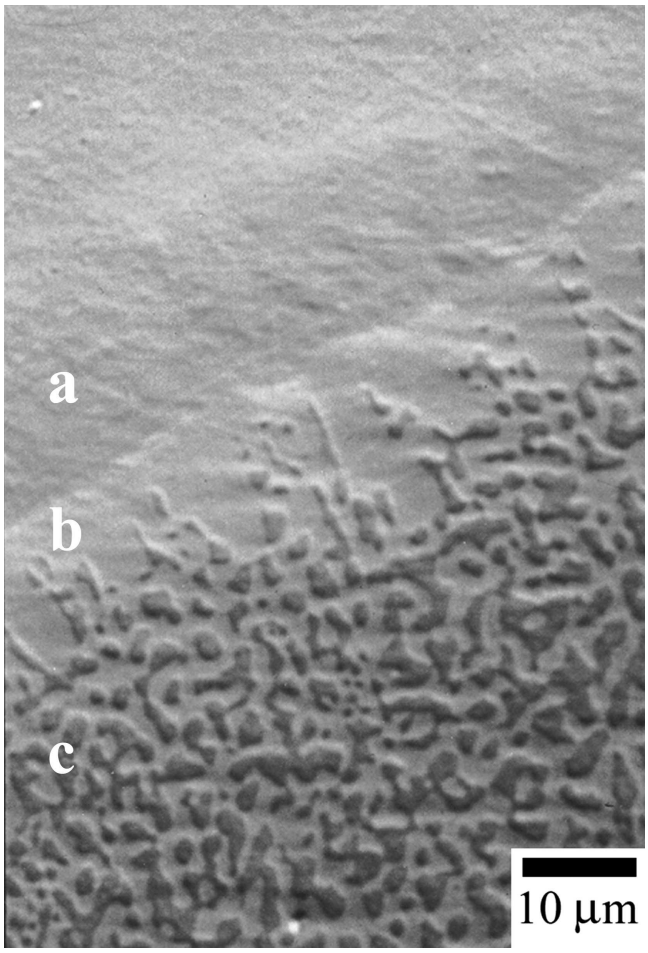

FIG. 3. Scanning electron microscopy image of the Au-rich diffusion couple. Using electron probe microanalysis, the phases present in this sample were determined to be (a) Au, (b) Au_5Sn, and the eutectic, (c) Au_5Sn + AuSn.

Figure 4 provides AFM-type images of the ζ' layer in the Au-rich diffusion couple. A large scale image (50 × 50 μm) shows the contrast from the Au to the ζ' layer to eutectic structure (29 at.% Sn) [compare with Fig. 4(a)]. In Fig. 4(b), a smaller scan of the ζ' layer where nanoindentation testing was conducted is shown. Images such as those in Fig. 4 were used for both the Au-rich and Sn-rich diffusion couples before and after nanoindentation testing. Overall, the phases tested in these two samples were: Au, Au_5Sn (ζ'), Au–Sn eutectic (29 at.% Sn), $AuSn_2$ (ϵ), $AuSn_4$ (η) and Sn. Table I lists the average and standard deviation for the collected measurements of indentation modulus and hardness measured for these materials by nanoindentation.

2. β-phase diffusion couple

The previously prepared diffusion couple[13] containing the β phase (8 at.% Sn) was also tested by nanoindentation. Prior to tests on the β phase, indents were performed in the pure Au and the Au rich alloy (10.0 at.% Sn) to characterize the properties of these starting materials. The tip was then placed at the interface, determined by sighting with an optical telescope. Testing for this sample was conducted by rastering the tip across the diffusion interface containing the β phase and indenting at approximately every 5–10 μm. This procedure was necessary as there was no obvious contrast indicating the boundaries of the β phase when pre-scanning with the AFM mode. Figure 5 presents the hardness measured for two profiles across the β phase, where the position was measured from AFM imaging of residual indents. The

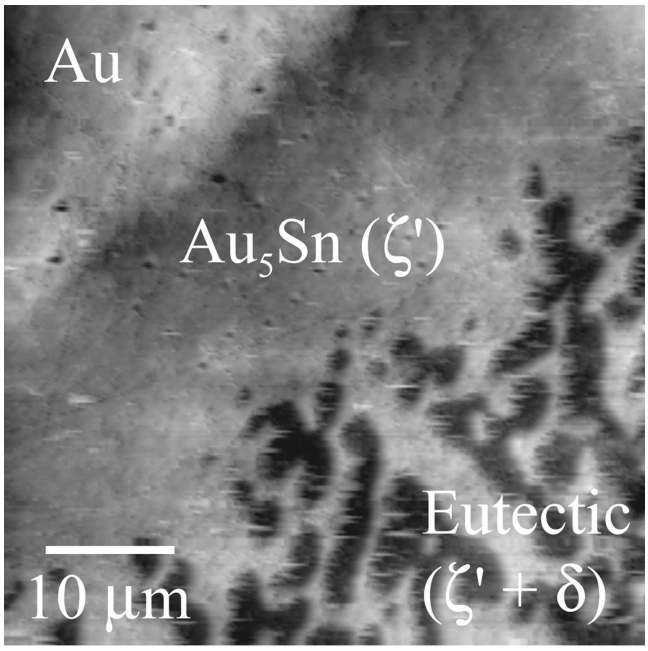

(a)

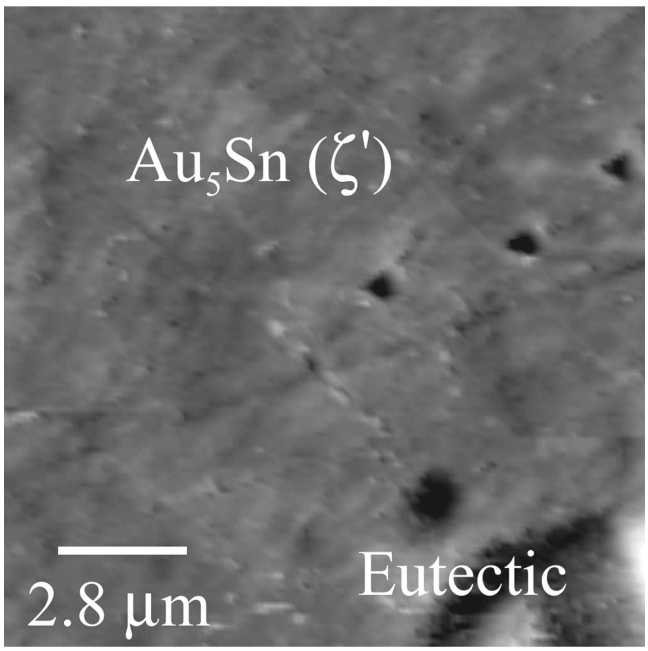

(b)

FIG. 4. Atomic force microscopy type images of the Au-rich diffusion couple generated by scanning with the nanoindenter tip. (a) For prescanning, the contrast observed between the Au, Au_5Sn, and the eutectic was sufficient to identify the tip position with respect to the various phases. (b) The indenter tip could then be placed at a specific position for testing followed by a post scan to observe residual indents.

TABLE I. Indentation modulus and hardness values for the materials tested by nanoindentation. The sample designation indicates the sample from which data was obtained: (a) Au-rich diffusion couple, (b) Sn-rich diffusion couple, (c) β phase diffusion couple, (d) AuSn bulk specimen, and (e) $(Au,Ni)Sn_4$ bulk specimen.

Material	Sample	Number of data points	Indentation modulus (GPa)	Hardness (GPa)
Au	a, b, c	28	95 ± 8	1.01 ± 0.09
Au	c	11	99 ± 7	1.05 ± 0.08
β (8 at.% Sn)	c	8	99 ± 9	1.24 ± 0.04
Au-rich alloy (10.0 at.% Sn)	c	9	86 ± 8	1.7 ± 0.1
Au_5Sn (ζ′)	a	19	91 ± 5	2.5 ± 0.2
Eutectic (ζ′ + δ)	a	6	88 ± 6	1.3 ± 0.2
AuSn (δ)	d	19	108 ± 9	1.4 ± 0.1
			96 ± 10[a]	1.1 ± 0.1[a]
$AuSn_2$ (ϵ)	b	19	108 ± 12	2.9 ± 0.4
$AuSn_4$ (η)	b	51	41 ± 8	1.2 ± 0.2
$(Au,Ni)Sn_4$	e	15	48 ± 3	1.8 ± 0.1
Sn	b	5	56 ± 5	0.25 ± 0.07

[a]Value is corrected for pileup.

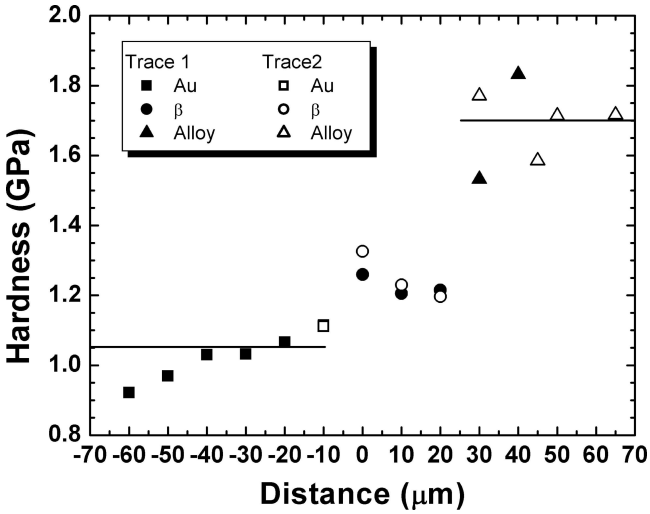

FIG. 5. Hardness versus position for nanoindentation tests in the β phase diffusion couple. The horizontal lines mark the average hardness values for Au and the Au-rich alloy tested far from the diffusion interface. Two hardness profiles are shown where symbols designate the materials tested: Au (square), β phase (circle), and Au-rich alloy (triangle).

measurements in the Au and Au-rich alloy corresponded well to measurements performed far from the interface, indicated by horizontal lines in Fig 5. A short plateau in the hardness, with values between the measurements for the other phases, exists in both profiles for a length of approximately 10–20 μm. The leftmost edge of this plateau is the zero point on the distance axis of the figure. This length measurement, corresponding to a thickness of the β phase, agrees well with what was measured previously for this sample.[13] The local trend of decreasing Au hardness with increasing distance from the interface is likely due to Sn dissolution in the Au, consistent with the phase diagram (Fig. 1). Data points obtained for the central region of the profiles in Fig. 5 were used to determine an average and standard deviation for the indentation modulus and hardness of the β phase. Table I lists this value along with average and standard deviations for the quasi-static mechanical properties measured for Au and the Au rich alloy in this diffusion couple.

3. Bulk samples: (Au,Ni)Sn_4 and AuSn

A total of twenty indentations were performed on the bulk AuSn (δ, 50.5 at.% Sn) sample. The residual indents in this alloy exhibited significant pileup, different from all other intermetallic compounds tested. Figure 6 is an AFM-type image of a residual indent in the AuSn sample. The bright features near the edge of the indent correspond to material pileup higher than the original surface. Profiles of the surface height (calculated from AFM data), along with traced images of the projected contact area were therefore used to determine the increase in contact area due to pileup. For all loads used to test this alloy (2.0–9.5 mN), the contact area corrected for pileup was roughly 25% greater than that measured from the tip area calibration on fused quartz. The average and standard deviation for the indentation modulus and hardness are presented in Table I for AuSn (δ), both as-measured and including the pileup correction. When including this correction, it is necessary to assume that the material pileup under maximum load is similar to the unloaded pileup observed for the residual indent.

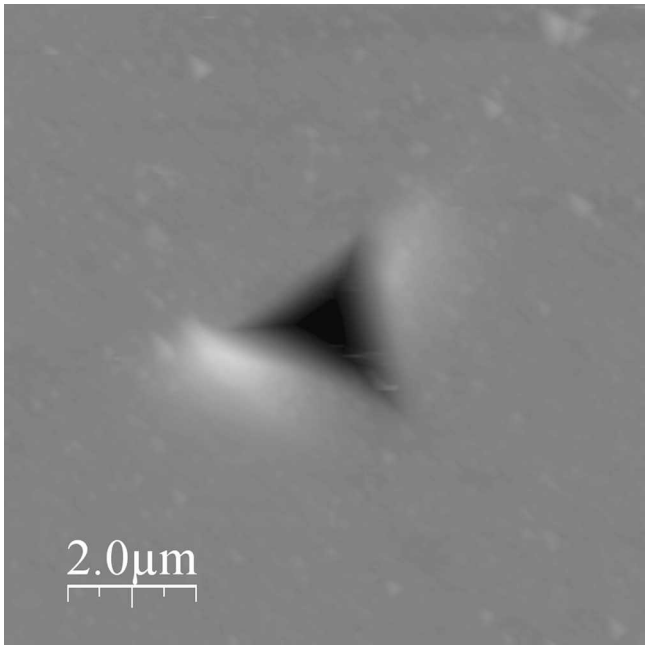

FIG. 6. Atomic force microscopy type image of residual indent from nanoindentation testing in the AuSn bulk sample.

Another feature of interest in Fig. 6 is the asymmetric nature of the pileup. This is due to plastic anisotropy in this particular compound. The AuSn phase has a hexagonal crystal structure, which is expected to exhibit anisotropic mechanical properties.[38–43] In an effort to understand the effects of anisotropy on the measured nanoindentation results, Vickers microhardness tests were performed on the AuSn sample. Figure 7 presents optical micrographs of two residual indents for Vickers testing, one for 1.96 N force [Fig 7(a)] and one for 9.8 N force [Fig 7(b)]. In one case, there is pileup similar to that observed in nanoindentation testing [Fig 7(b)], while in another there is no pileup [Fig 7(a)]. If the pileup is ignored in the calculation, the "deformed" Vickers indent has a hardness of 1.4 GPa, while that of the symmetric indent is 1.6 GPa. The nanoindentation hardness of 1.4 GPa, which is also uncorrected for pileup, matches well with the "deformed" Vickers indent. Electron backscatter diffraction was used to determine the crystalline orientation of the grains shown in Fig. 7. It was found that the symmetric indent occurred for loading along the *c* axis, while the asymmetric indent occurred for an arbitrary orientation lying more or less in the *a-b* plane. It appears that the nanoindentation testing was conducted in a grain that has an orientation more like the *a-b* plane than parallel to the *c* axis. Further work has been carried out on this alloy to quantify the plastic anisotropy in this intermetallic compound, primarily using Knoop indentation due to its enhanced sensitivity to crystalline anisotropy.[39,41] This work will appear in a separate publication.[44]

Nanoindentation was also performed on a bulk ingot of $Au_{0.5}Ni_{0.5}Sn_4$ alloy obtained from a previous study.[28] The sample was a single-phase alloy prepared by arc-melting followed by annealing. A total of 15 indentations were made on this specimen. The average and standard deviation for these measurements are presented in Table I. Unlike the AuSn bulk specimen, the $Au_{0.5}Ni_{0.5}Sn_4$ alloy was isotropic in response.

C. Nanoindentation creep

The room-temperature creep properties of Au–Sn eutectic (29 at.% Sn) and the individual intermetallic

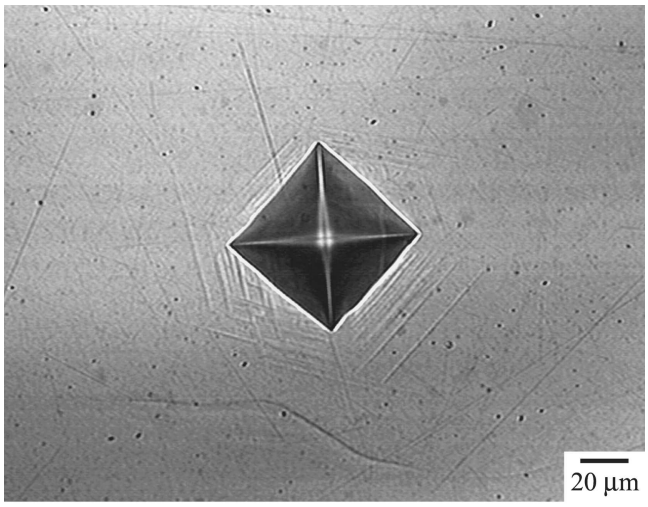

(a)

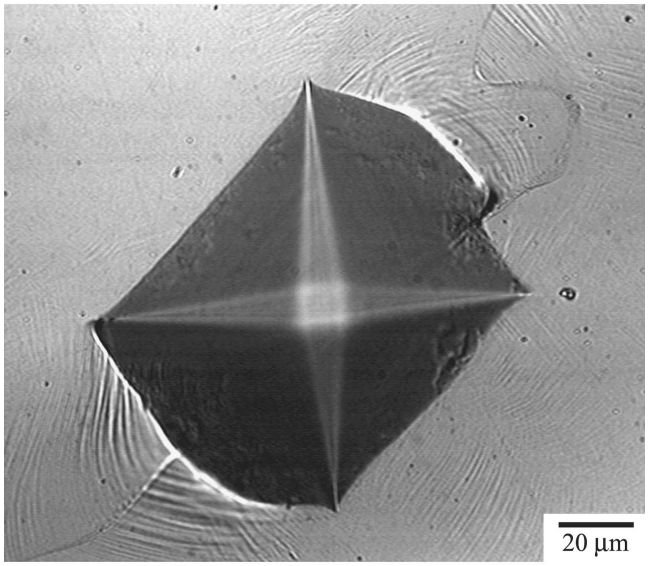

(b)

FIG. 7. (a) Light optical microscopy image of a residual indent from microindentation testing in the AuSn bulk sample. The load was 1.96 N. (b) Light optical microscopy image of residual indent from microindentation testing in the bulk AuSn sample.The load was 9.8 N.

phases (ζ'–Au_5Sn and δ–AuSn) that make this eutectic were investigated using load-controlled indentation. These experiments differ from the quasi-static indentation tests only in the length of the hold segments at maximum load (5–10 s), which were long enough that time-dependent relaxation could be explored. Strain rate versus stress curves are presented in Fig. 8 for creep of the three Au–Sn materials with a maximum indentation load of 1.0 or 2.0 mN. Also plotted in Fig. 8 for comparison are creep measurements on a pure Sn sample, In–Sn eutectic solder and a directionally solidified Sn–3.82 wt% Ag–0.9 wt% Cu eutectic alloy.[45,46] The indentation tests on the In–Sn specimen were conducted in the same manner outlined above. Creep measurements

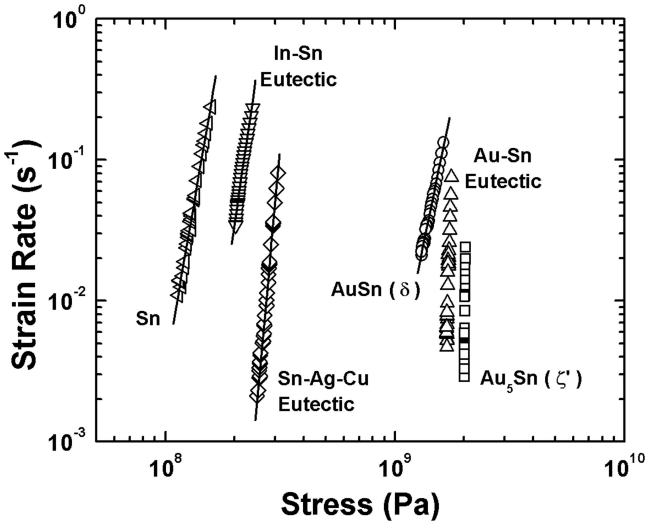

FIG. 8. A plot of strain rate versus hardness for Au–Sn eutectic and the constituent phases, Au_5Sn and AuSn. Also plotted is a creep measurements for Sn, In–Sn eutectic, and Sn–Ag–Cu eutectic.[46]

presented for pure Sn and the Sn–Ag–Cu eutectic were conducted with a load of 5 mN and hold segments of 30–60 s.

The length scale of indentations on the Au–Sn and In–Sn eutectic specimens were large enough to span multiple phase boundaries and were therefore considered to be measurements of the creep of the entire alloy rather than its constituent phases. In the case of the AuSn (δ), Au_5Sn (ζ'), and Sn measurements, these indents were performed in single phases. Finally, for the Sn–Ag–Cu specimen, the indent size (~10 μm across) was comparable to the scale of the microstructure.[45] Thus, the results from six tests performed in random locations were averaged to obtain an average creep behavior for this sample.

Linear regression was performed on the data presented in Fig. 8, where the slope corresponds to the creep exponent n [compare with Eq. (5)]. The fits for pure Sn ($n = 9$), In–Sn eutectic ($n = 11$), Sn–Ag–Cu eutectic ($n = 18$), and AuSn ($n = 8$) are shown in Fig. 8. These creep exponents are comparable to other indentation studies on solder and intermetallic compounds in solder joints. For example, Lucas et al.[34] measured $n = 11$ for a Sn–Ag solder and $n = 38$ for a much harder Cu–Sn intermetallic compound. Attempts to fit the results for the Au–Sn eutectic and Au_5Sn (ζ') yield even higher creep exponents, $n = 60$ for the Au–Sn eutectic and $n = 160$ for Au_5Sn. The physical meaning of these results would seem to be that these are materials with high creep resistance but also very high sensitivity to stress level. However, further examination of the creep rates for these two tests revealed that the rate of penetration of the indenter (~1 nm/s) was on the order of the drift rate of the nanoindentation system (~0.3 nm/s). Thus, we consider

our measurement of creep on these two materials as an upper limit, where the strain rate at the measured stresses may be even smaller, again indicating a very low creep rate. For tests on all of the other materials, the rate of penetration of the indenter was measured to be much greater [e.g., > 10 nm/s for In–Sn eutectic and ~5 nm/s for AuSn (δ)].

From the results presented in Fig. 8, it is apparent that the three materials used for soldering applications (Au–Sn, In–Sn and Sn–Ag–Cu eutectics) have distinctly different creep behavior. The Au–Sn eutectic and the constituent phases, AuSn (δ) and Au_5Sn (ζ′), all have enhanced creep properties in comparison to In–Sn eutectic and Sn–Ag–Cu eutectic. The stress needed to obtain a given creep strain rate in the Au–Sn phases is high as compared to the softer In–Sn and Sn–Ag–Cu solders; alternatively, at a given stress at which the creep rate in In–Sn or Sn–Ag–Cu is high, the creep rate in the Au–Sn phases is negligible (by extrapolation). These results are in apparent agreement with the melting points of these alloys, In–Sn eutectic (118 °C), Sn–Ag–Cu eutectic (~220 °C), and Au–Sn eutectic (280 °C), where the stress required for a given creep rate increases with increasing melting point. However, the creep rate of the Sn–Ag–Cu eutectic is much closer to that of the In–Sn eutectic, despite having a melting point closer to that of Au–Sn eutectic. The main difference between the Au–Sn eutectic and the other solder alloys is that it is a eutectic composed of two intermetallic phases, AuSn and Au_5Sn, which are both significantly harder than In or Sn. The Sn–Ag–Cu eutectic contains both Ag_3Sn and Cu_6Sn_5 intermetallics but is primarily Sn (~95 wt%). These measurements and comparisons support the common assertion that the Au–Sn eutectic is a hard solder with enhanced creep resistance in comparison to other common "soft" solders and imply that this particular characteristic is an inherent property of the materials rather than one of microstructure morphology. This implication is also supported by the fact that the creep behavior of the Au–Sn eutectic falls between that of its constituent phases. It is expected that a more traditional investigation of steady state creep on these solder materials would reveal the same differences in creep behavior observed here, but also indicate microstructural mechanisms that could be tied to long-term reliability.

D. Property and Literature Comparisons

1. Modulus

Comparisons of Young's modulus values for Au–Sn compounds are presented in Table II. The values tabulated for this work are determined from nanoindentation measurements and Eq. (2), where Poisson's ratio for a given intermetallic was either taken from the literature or assumed to be 0.33. For two of the phases studied here, β (8 at.% Sn) and $AuSn_2$, no measurements of Young's modulus were found in the literature. In the case of the other intermetallic compounds studied, a number of previous investigations were found and are presented for comparison in Table II. Yost et al. measured the elastic modulus and Poisson's ratio for ζ′, the eutectic (29 at.% Sn), and δ by resonance techniques.[15] Their measurements for the eutectic composition agree well with the values obtained here. However, for pure ζ′ and δ, the measurements of Yost et al. are consistently lower than those measured here. Vicenzo et al. measured moduli for electrodeposited Au–Sn compounds[18] with a range in composition (40–50 at.% Sn) over which they nominally deposited δ (50 at.% Sn). In the case of the δ phase in samples with 48–50 at.% Sn, they obtained a well-defined value of 101 ± 9 GPa somewhat higher than our value of 87 ± 9 GPa.

TABLE II. Young's modulus values for the Au–Sn intermetallics studied here along with values found in the literature for comparison.

Material	Young's modulus (GPa)	Poisson's ratio	Specimen/technique
β (8 at.% Sn)	88 ± 8	0.33[b]	This work
Au_5Sn (ζ′)	76 ± 5		This work
	62	0.4	Bulk, resonance[15]
Eutectic	74 ± 5		This work
	70	0.4	Bulk, resonance[15]
AuSn (δ)	87 ± 9[a]		This work
	71	0.3	Bulk, resonance[15]
	101 ± 9		Thick film, micro-indentation[18]
$AuSn_2$ (ϵ)	103 ± 9	0.33[b]	This work
$AuSn_4$ (η)	39 ± 4		This work
	71	0.31	Bulk, resonance[16]
$(Au,Ni)Sn_4$	48 ± 3	0.33[b]	This work

[a]Value is corrected for pileup.
[b]Value for Poisson's ratio is assumed.

For the intermetallic compound $AuSn_4$, Ghosh measured a Young's modulus using resonance techniques.[16] In the past, our nanoindentation measurements have been found to be higher than those determined by resonance,[22] including comparisons to Ghosh's measurements on Cu–Sn and Ag–Sn compounds.[16] However, the value measured by resonance for $AuSn_4$, 71 GPa, is much higher than that determined from our nanoindentation measurements, 39 ± 4 GPa. One possible reason for such a large discrepancy would be if the $AuSn_4$ compound exhibited significant anelasticity. Relaxation mechanisms with small, but measurable time constants, may be sampled during a nanoindentation test but would have a negligible effect on a measurement using ultrasonic techniques. To investigate this possibility, the unloading rate during nanoindentation was varied between 0.01 and 2.0 mN/s. This range of unloading rates has been seen to be sensitive to anelasticity in pure Sn in the past,[47] resulting in a lower modulus for slower unloading rates. For our tests

on the $AuSn_4$ compound, however, no dependence of the modulus on unloading rate was observed. A second possible reason for the difference in modulus between Ghosh and this work could be related to a significant anisotropy in the mechanical properties of the $AuSn_4$ compound. However, even if this were true, sampling of anisotropic effects via nanoindentation is generally muted due to the non-uniaxial nature of the test.[48,49] Thus, the large difference between the measurement by Ghosh and that determined here can only be ascribed to differences in technique.

2. Hardness

The hardness values for the Au–Sn intermetallic compounds are compared to literature values in Table III. Comparisons are made for all of the alloys studied. Ciulik and Notis reported values for Au–Sn intermetallic compounds measured by Vickers microindentation using a force of 0.49 N.[17] Vicenzo et al. also measured hardness for the AuSn phase by large load nanoindentation,[18] finding a value of 2.1 GPa. This is much higher than the hardness measured here and by Ciulik and Notis. It is possible the small grain size in their electrodeposited films resulted in some strengthening. The discrepancies in the measurements in the AuSn phase could also be due to anisotropy effects. For the β phase, our measurements agree reasonably well with Cuilik and Notis, with our numbers only slightly lower. In the case of the ζ′, δ, and ϵ compounds, our measurements are higher than those measured in their study. Given that the penetration depth associated with nanoindentation is very small, it is possible that the Au_5Sn and $AuSn_2$ intermetallics exhibit a significant indentation size effect, similar to that seen in the high-hardness Cu_6Sn_5 intermetallic.[22] Ghosh measured the hardness of $AuSn_4$ by microindentation to be 0.63 GPa.[16] Compared to our 1.2 GPa measured with smaller loads, it appears there may be an indentation size effect for this compound as well. Ghosh typically observed fracture when indenting this compound, an event we did not observe. This specific difference in behavior between micro- and nanoindentation has been found in the past to lead to an indentation size effect in intermetallic compounds.[22]

TABLE III. Hardness values for the Au–Sn intermetallic compounds studied here along with values from the literature for comparison.

Material	Hardness (GPa)	Specimen/technique
β (8 at.% Sn)	1.24 ± 0.04	This work
	1.32 ± 0.04	Bulk, Vickers[17]
Au_5Sn (ζ′)	2.5 ± 0.2	This work
	1.33 ± 0.05	Bulk, Vickers[17]
AuSn (δ)	1.1 ± 0.06[a]	This work
	1.54 ± 0.04	Bulk, Vickers[17]
	2.1 ± 0.2	Thick film, micro-indentation[18]
$AuSn_2$ (ϵ)	2.9 ± 0.4	This work
	2.18 ± 0.04	Bulk, Vickers[17]
$AuSn_4$ (η)	1.2 ± 0.2	This work
	0.63 ± 0.06	Bulk, Vickers[16]

[a]Value is corrected for pileup.

E. Role of Au in soldering applications

The use of Au in soldering is due to its good oxidation and corrosion resistance. Thus, it is commonly used for pad metallurgies to protect an underlying layer of Ni or Cu. However, over the years it has been recognized that solder joints with significant amounts of Au tend to be mechanically weak after thermal aging or cycling. This is often attributed to the formation of the $AuSn_4$ compound that typically appears at the solder/metallization interface.[7,10,11] In the case of Ni/Au pad metallurgies, this compound is actually an $(Au,Ni)Sn_4$ compound. Despite significant effort to solve the problem of Au embrittlement, little has been known about the mechanical properties of $AuSn_4$ and $(Au,Ni)Sn_4$. However, it has been hypothesized that these materials are inherently brittle. Figure 9 is a comparison of the load versus displacement curves measured by nanoindentation for the $AuSn_4$, $(Au,Ni)Sn_4$, $AuSn_2$ intermetallics measured here and the Cu_6Sn_5 and Cu_3Sn intermetallics measured previously.[22] It can be seen that the $AuSn_4$ and $(Au,Ni)Sn_4$ compounds deform more for a given load, have shallower unloading slopes, and larger residual indentation depths. Thus, they have a lower hardness, lower modulus, and are more ductile than the Cu–Sn compounds commonly found in reliable solder joints. In fact, even the hardest Au–Sn compound in our study, $AuSn_2$, is more ductile than the Cu–Sn compounds (Fig. 9). Also, a recent report has also demonstrated that the coefficients of thermal expansion of $AuSn_4$ and $(Au,Ni)Sn_4$ are in a desirable range for

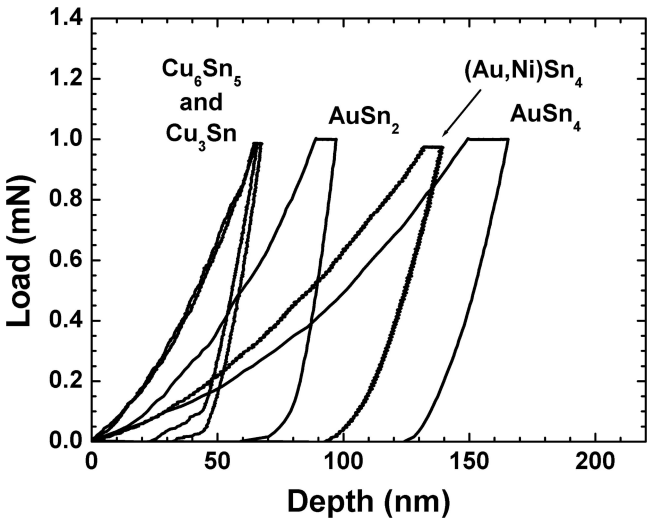

FIG. 9. Load versus displacement curves for nanoindentation testing of Cu–Sn and Au–Sn intermetallic compounds.

solder joint applications.[50] Therefore, these Au-containing intermetallic compounds have fundamental properties similar to, or better than, other materials that are found in reliable solder joints.

In the recent work of Alam et al. detailing a pad metallurgy for reduced Au embrittlement,[7] the thickness of Ni was reduced in the Cu/Ni/Au metallization stack. This resulted in the formation of a $(Cu,Ni)_6Sn_5$ compound and nodules of $AuSn_4$. This changed a number of parameters associated with the common interface composition of a Ni/Au joint that results in brittle failure with aging [see Fig 10(a)]. First, the $(Au,Ni)Sn_4$ compound changed to $AuSn_4$ and became an incomplete, noduled layer rather than a uniform growth layer. Second, a $(Cu,Ni)_6Sn_5$ compound grew at the interface instead of Ni_3Sn_4. Alam et al. attributed the enhanced strength to the change in the composition of the Au-containing intermetallic.[7] Specifically they indicated that the $AuSn_4$ phase is likely less brittle than the $(Au,Ni)Sn_4$ phase. Our study agrees with this hypothesis, indicating a reduction in hardness of 1.8 to 1.2 GPa in going from $(Au,Ni)Sn_4$ to $AuSn_4$. However, if one considers the hardness of Cu_6Sn_5 is on the order of 6.0 GPa, both $AuSn_4$ and $(Au,Ni)Sn_4$ are quite soft by comparison. In addition, one cannot neglect instances in the literature of $AuSn_4$ growth layers resulting in brittle failure.[2,8,9] Thus, it does not seem likely that the composition change is completely responsible for the improvement in strength observed by Alam et al., leading to the consideration of other factors.[7]

A challenge in finding an explanation for the discrepancy between the high reliability one would expect based on the mechanical properties measured here and the reality of Au embrittlement in actual joints is the lack of a concrete determination of failure mechanisms in solder joints containing Au. It is exceedingly difficult to trace a solder joint failure to a specific root cause. In comparing the strength of different solder joints, one must consider the possibility that the behavior may be due not to the intermetallic compositions and properties, but to the interface morphology. In the work of Pratt et al.,[51] it was demonstrated that excessive growth of Cu_6Sn_5 and Cu_3Sn compounds will also result in decreased strength of solder joints and brittle failure at the interface. Thus, in at least two instances, a single continuous layer, with a scalloped or noduled layer proves reliable, but a multilayered interface proves unreliable. This is shown schematically in Figs. 10(a) and 10(b). On the top, solder joints with an interface consisting of two intermetallic phases with one layer incomplete or scalloped proved generally reliable. On the bottom, solder joints with a multilayer of two intermetallics of considerable thickness (>1 μm) prove weak, brittle, and unreliable.

From this discussion, it is clear that not only the properties of the phases, but also their morphologies, are important. Based on our measurement of the properties of $AuSn_4$ and $(Au,Ni)Sn_4$ phases, it appears that the brittleness of Au-containing joints is more likely to come from a problem of interface strength and microstructural effects rather than the mechanical properties of the

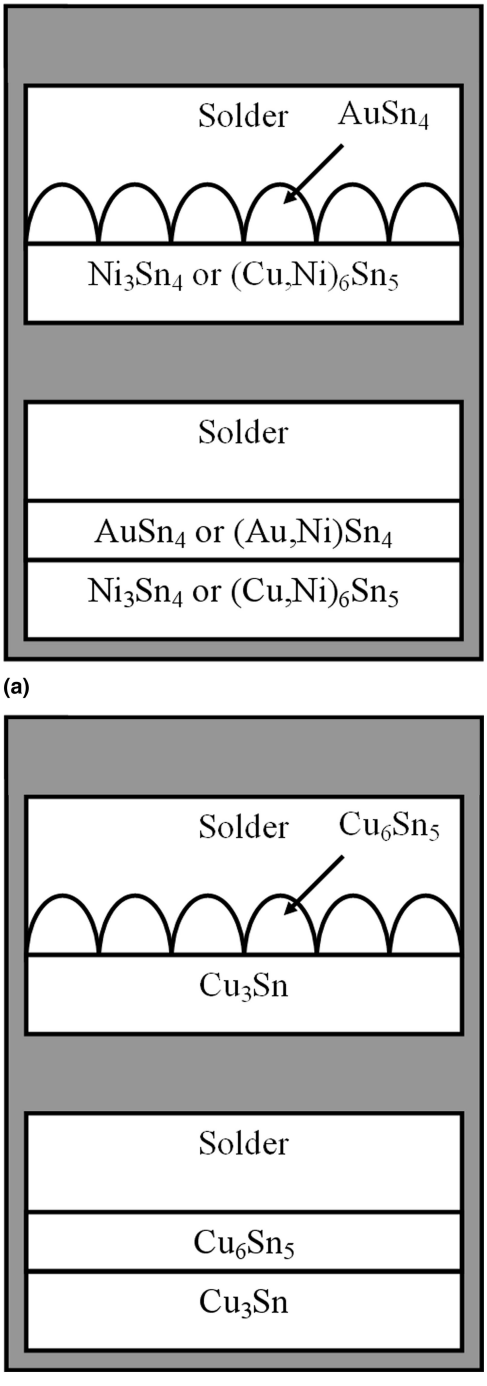

FIG. 10. Examples of interface microstructures for (a) Au containing solder joints and (b) solder bonded to Cu. The scalloped or noduled microstructures on the top half are generally reliable, resulting in acceptable joint strength and lifetimes. The multilayered microstructures on the bottom are found to be unreliable with decreased joint strength and lifetimes.

intermetallic compounds themselves. The multilayered structure of two intermetallics appears to be specifically weak, regardless of the phases of interest. To clearly identify the cause for failure, measurements of interface strength between the intermetallics of interest would be helpful. As solder joints become smaller, the understanding of failure mechanisms at this level of detail is likely to become more important.

IV. CONCLUSIONS

Quasi-static elastic and plastic properties have been determined for all room temperature Au–Sn intermetallics, the β phase (8 at.% Sn), $AuSn_4$, and $(Au,Ni)Sn_4$ using a single experimental technique, nanoindentation. Time-dependent behavior was explored by indentation creep measurements for the Au–Sn eutectic (29 at.% Sn) and its constituent phases. The elastic moduli and hardness values of Au–Sn compounds are similar to, or smaller than, those of Cu–Sn intermetallics common to many solder joints. Thus, the Au–Sn intermetallics are rather ductile by comparison. In particular, the $AuSn_4$ and $(Au,Ni)Sn_4$ phases, commonly blamed for Au embrittlement of solder joints, were found to be relatively soft with hardness values of 1.2 GPa and 1.8 GPa, respectively. This result points to the likelihood of microstructural and interface strength effects as the root cause for Au embrittlement, not the properties of the intermetallic compounds themselves. The Au_5Sn (ζ′) and AuSn (δ) intermetallics were found to have hardness values greater than those of typical soft solders, and higher stress was required to induce similar creep rates to In–Sn or Sn–Ag–Cu eutectic solders. Thus, the creep properties of Au–Sn eutectic solder, which is comprised of these two intermetallics, should be enhanced in comparison to other solders as is commonly observed, and is therefore an inherent property of the materials.

ACKNOWLEDGMENTS

We gratefully acknowledge financial support from The Center for Optical Technologies, Lehigh University, Bethlehem, PA. The $(Au,Ni)Sn_4$ sample was graciously prepared and donated to us by Lubov Zavalij at SUNY-Binghamton, Binghamton, NY.

REFERENCES

1. J. Whitfield and A.J. Cubbin: Experimental observations on the effect of gold and palladium on soldered joints. Plating (East Orange, New Jersey). **52,** 889 (1965).
2. F. Gordon Foster: Embrittlement of solder by gold from plated surfaces. *ASTM Special Tech. Pub.* **319,** 13 (1962).
3. H. Mavoori: Dimensionally stable solders for optoelectronics and microelectronics. *JOM* **52**(6), 29 (2000).
4. C.H. Zhong and S. Yi: Solder joint reliability of plastic ball grid array packages. *Solder. Surf. Mount Technol.* **11**(1), 44 (1999).
5. Z. Mei and A. Eslambolchi: Evaluation of Ni/Pd/Au as an alternative metal finish on PCB. *Circuit World* **25**(2), 18 (1999).
6. Z. Mei, M. Kaufmann, A. Eslambolchi, and P. Johnson: Brittle interfacial fracture of PBGA packages soldered on electroless nickel/immersion gold, in *Proceedings—Electronic Components & Technology Conference,* Vol. 48 (IEEE, New York, NY, 1998), pp. 952–961.
7. M.O. Alam, Y.C. Chan, and K.N. Tu: Elimination of Au-embrittlement in solder joints on Au/Ni metallization. *J. Mater. Res.* **19,** 1303 (2004).
8. M.R. Marks: Effect of burn-in on shear strength of 63Sn–37Pb solder joints on an Au/Ni/Cu substrate. *J. Electron. Mater.* **31,** 265 (2002).
9. D.H. Daebler: An overview of gold intermetallics in solder joints. *Surf. Mount Technol.* **5**(10), 43 (1991).
10. A.M. Minor and J.W. Morris, Jr.: Growth of a Au-Ni-Sn intermetallic compound on the solder-substrate interface after aging. *Metall. Mater. Trans.* **31A,** 798 (2000).
11. A. Zribi, R.R. Chromik, R. Presthus, K. Teed, L. Zavalij, J. DeVita, J. Tova, E.J. Cotts, J.A. Clum, R. Erich, A. Primavera, G. Westby, R.J. Coyle, and G.M. Wenger: Solder metallization interdiffusion in microelectronic interconnects. *IEEE Trans Components Packaging Technol.* **23,** 383 (2000).
12. A. Zribi, R.R. Chromik, R. Presthus, J. Clum, K. Teed, L. Zavalij, J. DeVita, J. Tova, and E.J. Cotts: Solder metallization interdiffusion in microelectronic interconnects, in *49th Electronic Components and Technology Conference* (IEEE, New York, NY, 1999), pp. 451–457.
13. J. Ciulik and M.R. Notis: The Au–Sn phase diagram. *J. Alloys Compd.* **191**(1), 71 (1993).
14. J.R. Ciulik: An experimental determination of the Au-rich portion of the Au–Sn phase diagram. Masters Thesis, Lehigh University, Bethlehem, PA (1988).
15. F.G. Yost, M.M. Karnowsky, W.D. Drotning, and J.H. Gieske: Thermal expansion and elastic properties of high gold-tin alloys. *Metall. Trans.* **21A,** 1885 (1990).
16. G. Ghosh: Elastic properties, hardness, and indentation fracture toughness of intermetallics relevant to electronic packaging. *J. Mater. Res.* **19,** 1439 (2004).
17. J. Ciulik and M.R. Notis: Phase equilibria and physical properties in the Au–Sn system, in *Microelectronic Packaging Technology, Materials and Processes,* Proceedings of the 2nd ASM International Electronic Materials and Processing Congress (ASM International, Materials Park, OH, 1989), pp. 57–61.
18. A. Vicenzo, M. Rea, L. Vonella, M. Bestetti, and P.L. Cavallotti: Electrochemical deposition and structural characterization of Au–Sn alloys. *J. Solid State Electrochem.* **8**(3), 159 (2004).
19. R.J. Fields, S.R. Low III, and G.K. Lucey, Jr.: Physical and mechanical properties of intermetallic compounds found in solder joints, in *The Metal Science of Joining*, edited by M.J. Cieslak, J.H. Perepezko, S. Kang, and M.E. Glicksman (TMS, Warrendale, PA, 1991), pp. 165–174.
20. W.K. Warburton and D. Turnbull: Fast diffusion in metals, in *Diffusion in Solids: Recent Developments*, edited by A.S. Nowick and J.J. Burton (Academic Press, New York, 1975), pp. 171–229.
21. R.R. Chromik and E.J. Cotts: Thermodynamic and kinetic study of phase transformations in solder/metal systems, in *Electronic Packaging Materials Science IX*, edited by S.K. Groothuis, P.S. Ho, K. Ishida, and T. Wu (Mater. Res. Soc. Symp. Proc. **445,** Pittsburgh, PA, 1997), pp. 31–36.
22. R.R. Chromik, R.P. Vinci, S.L. Allen, and M.R. Notis: Nanoindentation measurements on Cu–Sn and Ag–Sn intermetallics formed in Pb-free solder joints. *J. Mater. Res.* **18,** 2251 (2003).
23. X. Deng, M. Koopman, N. Chawla, and K.K. Chawla: Young's

modulus of (Cu, Ag)-Sn intermetallics measured by nanoindentation. *Mater. Sci. Eng. A* **A364**(1–2), 240 (2004).
24. X. Deng, N. Chawla, K.K. Chawla, and M. Koopman: Deformation behavior of (Cu, Ag)–Sn intermetallics by nanoindentation. *Acta Mater.* **52,** 4291 (2004).
25. G.Y. Jang, J.W. Lee, and J.G. Duh: The nanoindentation characteristics of Cu_6Sn_5, Cu_3Sn, and Ni_3Sn_4 intermetallic compounds in the solder bump. *J. Electron. Mater.* **33,** 1103 (2004).
26. N. Chawla, B.V. Patel, M. Koopman, K.K. Chawla, R. Saha, B.R. Patterson, E.R. Fuller, and S.A. Langer: Microstructure-based simulation of thermomechanical behavior of composite materials by object-oriented finite element analysis. *Mater. Charact.* **49,** h395 (2002).
27. D. Tabor: *The Hardness of Metals* (Oxford University Press, Oxford, U.K., 1951), pp. 67–83.
28. L. Zavalij, A. Zribi, R.R. Chromik, S. Pitely, P.Y. Zavalij, and E.J. Cotts: Crystal structure of $Au_{1-x}Ni_xSn_4$ intermetallic alloys. *J. Alloys Compd.* **334,** 79 (2002).
29. A. Paul, A.A. Kodentsov, and J.J. van Loo: Intermetallic growth and Kirkendall effect manifestations in Cu/Sn and Au/Sn diffusion couples. *Z. Metallkde.* **10,** 913 (2004).
30. W.C. Oliver and G.M. Pharr: An improved technique for determining hardness and elastic modulus using load and displacement sensing indentation experiments. *J. Mater. Res.* **7,** 1564 (1992).
31. B.N. Lucas and W.C. Oliver: Indentation power-law creep of high-purity indium. *Metall. Mater. Trans. A* **30A,** 601 (1999).
32. M.J. Mayo and W.D. Nix: A micro-indentation study of superplasticity in Pb, Sn, and Sn-38 wt% Pb. *Acta Metall.* **36,** 2183 (1988).
33. J.P. Lucas, A.W. Gibson, K.N. Subramanian, and T.R. Bieler: Nanoindentation characterization of microphases in Sn-3.5 Ag eutectic solder joints, in *Fundamentals of Nanoindentation and Nanotribology,* edited by N.R. Moody, W.W. Gerberich, N. Burnham, and S.P. Baker (Mater. Res. Soc. Symp. Proc. **522,** Warrendale, PA, 1998), p. 339.
34. J.P. Lucas, H. Rhee, F. Guo, and K.N. Subramanian: Mechanical properties of intermetallic compounds associated with Pb-free solder joints using nanoindentation. *J. Electron. Mater.* **32,** 1375 (2003).
35. A.C. Fischer-Cripps: *Nanoindentation* (Springer, New York, 2002), pp.126–141.
36. T.Y. Tsui, J. Vlassak, and W.D. Nix: Indentation plastic displacement field: Part II. The case of hard films on soft substrates. *J. Mater. Res.* **14,** 2204 (1999).
37. T.Y. Tsui, J. Vlassak, and W.D. Nix: Indentation plastic displacement field: Part I. The case of soft films on hard substrates. *J. Mater. Res.* **14,** 2196 (1999).
38. K.C. Yoo, J.A. Spitznagel, and R.H. Hopkins: Studies on the plastic-deformation of Tl_3AsSe_3 single-crystals by hardness indentation. *J. Mater. Res.* **3,** 1404 (1988).
39. C.A. Brookes, J.B. Oneill, and B.A.W. Redfern: Anisotropy in hardness of single crystals. *Proc. R. Soc. London A, Math. Phys. Sci.* **322,** 73 (1971).
40. F.W. Daniels and C.G. Dunn: The effect of orientation on Knoop hardness of single crystals of zinc and silicon ferrite. *Trans. Am. Soc. Metals* **41,** 419 (1949).
41. D. Lee: Plasticity considerations for anisotropic materials in hardness indentation, in *The Science of Hardness Testing and Its Research Applications*, edited by J.H. Westbrook and H. Conrad (ASM, Metals Park, OH, 1971), pp. 147–166.
42. P.G. Riewald and L. Vanvlack: Deformation and fracture of MeTe and MnSe/MnTe solid solutions. *J. Am. Ceram. Soc.* **53,** 219 (1970).
43. F.W. Vahldiek and S.A. Mersol: Slip and microhardness of IVa to VIa refractory materials. *J. Less-Common Met.* **55,** 265 (1977).
44. R.R. Chromik, A. Shugar, R.P. Vinci, M.R. Notis: Plastic anisotropy of AuSn studied by indentation (unpublished).
45. S.L. Allen, M.R. Notis, R.R. Chromik, R.P. Vinci, D.J. Lewis, and R. Schaefer: Microstructural evolution in lead-free solder alloys: Part II. Directionally solidified eutectic Sn–Ag–Cu, Sn–Cu, and Sn–Ag alloys. *J. Mater. Res.* **19,** 1425 (2004).
46. R.R. Chromik (unpublished work, Lehigh University, Bethlehem, PA, 2004).
47. R.R. Chromik (unpublished work, Lehigh University, Bethlehem, PA, 2004).
48. J.J. Vlassak and W.D. Nix: Measuring the elastic properties of anisotropic materials by means of indentation experiments. *J. Mech. Phys. Solids* **42,** 1223 (1994).
49. J.J. Vlassak and W.D. Nix: Indentation modulus of elastically anisotropic half spaces. *Philos. Mag. A* **67,** 1045 (1993).
50. S. Pitely, L. Zavalij, S. Zarembo, and E.J. Cotts: Linear coefficients of thermal expansion of $Au_{0.5}Ni_{0.5}Sn_4$, $Au_{0.75}Ni_{0.25}Sn_4$, and $AuSn_4$. *Scripta Mater.* **51,** 745 (2004).
51. R.E. Pratt, E.I. Stromswold, and D.J. Quesnel: Effect of solid-state intermetallic growth on the fracture toughness of Cu/63Sn-37Pb solder joints. *IEEE Trans. Components, Packaging, Manufacturing Technol. A* **19,** 134 (1996).